



## Spin reorientation to a $\Gamma_3(C_x, F_y, A_z)$ configuration and anisotropic spin-phonon coupling in a $\text{Sm}_{0.5}\text{Y}_{0.5}\text{FeO}_3$ single crystal

Bhawana Mali <sup>1,\*</sup>, Janaky Sunil,<sup>2,†</sup> Harikrishnan S. Nair,<sup>3</sup> Chandrabhas Narayana <sup>2</sup> and Suja Elizabeth<sup>1</sup>

<sup>1</sup>Department of Physics, Indian Institute of Science, Bangalore, Karnataka 560012, India

<sup>2</sup>Chemistry and Physics of Materials Unit, Jawaharlal Nehru Centre for Advanced Scientific Research, Jakkur P.O., Bangalore 560064, India

<sup>3</sup>Department of Physics, 500 W. University Ave., The University of Texas at El Paso, El Paso, Texas 79968, USA



(Received 29 October 2021; revised 4 April 2022; accepted 1 June 2022; published 14 June 2022)

An unusual temperature-induced spin reorientation transition from  $\Gamma_2(F_x, C_y, G_z)$ - $\Gamma_{23}$ - $\Gamma_3(C_x, F_y, A_z)$  in orthoferrite  $\text{Sm}_{0.5}\text{Y}_{0.5}\text{FeO}_3$  is observed in the range 282–312 K through magnetic susceptibility measured on oriented single crystals. The  $\Gamma_2$ - $\Gamma_{23}$ - $\Gamma_3$  transition is distinctly different from the spin configurations commonly observed in  $R\text{FeO}_3$  orthoferrites, and we corroborate the finding with results from Raman spectroscopic investigations. Observation of magnon spectra and the vivid correlation between spin reorientation and changes in  $B_{2g}$  and  $B_{3g}$  phonon modes unveil strong spin-phonon coupling prevalent in  $\text{Sm}_{0.5}\text{Y}_{0.5}\text{FeO}_3$  crystal.

DOI: [10.1103/PhysRevB.105.214417](https://doi.org/10.1103/PhysRevB.105.214417)

### I. INTRODUCTION

Orthoferrites of the type  $R\text{FeO}_3$  ( $R$  = rare earth) belong to a family of canted antiferromagnets which crystallize in distorted perovskite structure with  $Pbnm$  space group [1].  $R\text{FeO}_3$  compounds have generated interest in the last few years due to their practical applications such as ultrafast spin switching [2], temperature and field-induced spin reorientation transitions, magnetization reversal [3], and multiferroicity [4]. The  $R$  and Fe magnetic sublattices in  $R\text{FeO}_3$  give rise to three types of competitive magnetic interactions, namely,  $R^{3+}$ - $R^{3+}$ ,  $R^{3+}$ - $\text{Fe}^{3+}$ , and  $\text{Fe}^{3+}$ - $\text{Fe}^{3+}$ . The  $\text{Fe}^{3+}$ - $\text{Fe}^{3+}$  interaction is the strongest, and is responsible for the noncollinear antiferromagnetic (AFM) ordering of Fe spins which lead to high Néel temperatures  $T_N \sim 600$ – $700$  K [1]. A weak ferromagnetic (FM) moment results due to the canted AFM ordering of Fe spins below  $T_N$  resulted from Dzyaloshinskii-Moriya interactions. The rare-earth sublattice polarizes in the molecular field of  $\text{Fe}^{3+}$  sublattice, and the anisotropic  $R^{3+}$ - $\text{Fe}^{3+}$  interaction induces a spin reorientation (SR) of Fe sublattice leading to the rotation of the weak FM component from one crystallographic axis to another. SR transition is initiated by strong  $4f$  magnetic anisotropy which depends on the population of  $4f$  electrons in different sublevels of the ground-state multiplet [5]. It is associated with a large orbital magnetic moment and can vary strongly via thermal occupancy changes in the  $4f$  orbital levels. Since  $\text{Fe}^{3+}$  has a half-filled  $3d$  shell exhibiting only a small magnetic single-ion anisotropy, the weak interaction between  $4f$ - $3d$  shells can influence the magnetic easy axis [6].

Among all possible spin configurations for  $R\text{FeO}_3$  compounds  $\Gamma_3(C_x, F_y, A_z)$  spin configuration was considered inconsistent with strong antiferromagnetic coupling observed

between nearest Fe neighbors and was not observed in the orthoferrites [1]. But, recently,  $\Gamma_3$  configuration was observed in  $\text{Er}_{0.6}\text{Dy}_{0.4}\text{FeO}_3$  [7], where doping with Dy alters the bond and lattice parameters in a manner that renders the AFM coupling between nearest  $\text{Fe}^{3+}$  neighbors relatively weak. The weak AFM coupling between  $\text{Fe}^{3+}$  sublattices helps in aligning the  $C$ -type and  $A$ -type AFM components along  $a$  and  $c$  axes rather than a strong  $G$  type. This results in weak ferromagnetism along the  $b$  axis [7]. The  $R^{3+}$  sublattice is AFM ordered at low temperature,  $T < 10$  K, due to weak  $R^{3+}$ - $R^{3+}$  interactions. Spin reorientation transition is observed in  $R\text{FeO}_3$  compounds, only when  $R$  is magnetic. The spin reorientation temperature ( $T_{\text{SR}}$ ) for  $R\text{FeO}_3$  compounds varies in the range of 10–480 K [1].

Among various members of the  $R\text{FeO}_3$  family,  $\text{SmFeO}_3$  is a widely studied compound as it shows excellent device characteristics such as fast magnetic switching [8] and spin reorientation transition from  $\Gamma_4(G_x, A_y, F_z)$  to  $\Gamma_2(F_x, C_y, G_z)$  spin configuration at high temperatures ( $T_{\text{SR1}} = 450$  K and  $T_{\text{SR2}} = 480$  K) [1,9]. It possesses the highest  $T_{\text{SR}}$  in the entire  $R\text{FeO}_3$  family and is consequently the focus of special attention in practical applications. Further,  $\text{SmFeO}_3$  is known to exhibit spontaneous magnetization reversal below 4 K [9], which is interpreted as long-range ordering of  $\text{Sm}^{3+}$  spins where the net magnetic moment is antiparallel to the weak ferromagnetic moment in the  $\text{Fe}^{3+}$  sublattice [9]. Further,  $\text{YFeO}_3$  exhibits  $G$ -type antiferromagnetism with  $T_N = 645$  K. The  $\text{Fe}^{3+}$  spins are ordered in  $\Gamma_4(G_x, A_y, F_z)$  configuration and remain in  $\Gamma_4$  until low temperature [1] and unlike  $\text{SmFeO}_3$ , does not exhibit any temperature-induced SR transition as Y is nonmagnetic. However, field-driven spin reorientation is observed at about 4 T [10].

In this work, we report the results of magnetic and Raman spectroscopic studies on oriented single crystals of  $\text{Sm}_{0.5}\text{Y}_{0.5}\text{FeO}_3$  which unveil a temperature-induced spin reorientation to  $\Gamma_3(C_x, F_y, A_z)$  magnetic configuration which is not commonly observed in orthoferrites. Signatures of strong

\*bhawana@iisc.ac.in

†janaky@jncasr.ac.in

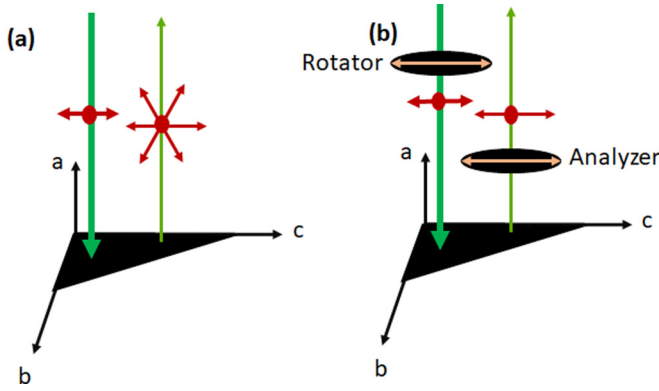


FIG. 1. Schematic showing the orientation and polarization direction of incident and scattered light for (a) standard Raman experiment and (b) polarized Raman experiment on (100)-plane oriented  $\text{Sm}_{0.5}\text{Y}_{0.5}\text{FeO}_3$  single crystal.

spin-phonon coupling leading to this transition is evidenced through Raman spectroscopy.

## II. EXPERIMENTAL METHODS

The details of single-crystal preparation of  $\text{Sm}_{0.5}\text{Y}_{0.5}\text{FeO}_3$  and its structural characterization using x-ray diffraction are given in the Supplemental Material (SM) [11] (see, also, Refs. [12–15] therein). The cleaved plate  $\perp$  to  $a$  axis is defined as (100) plane and that  $\perp$  to  $b$  axis is defined as (010) plane. Magnetization was measured in the temperature range of 5–400 K. An external field of 20 Oe was applied for zero-field (ZF), field-cooling (FC), and field-warming (FW) protocols. Magnetic measurements were also performed in the high-temperature range of 400 to 800 K at 50 Oe external field in both zero-field-cooled (ZFC) and field-cooled warming (FCW) protocols using physical property measurement system (PPMS) (Quantum Design). Isothermal magnetization (MH) up to  $\pm 70$  kOe was measured using Quantum Design Superconducting Quantum Interference Device (SQUID). Raman spectroscopy data were collected using a Horiba (Labram HR Evolution) micro Raman spectrometer equipped with Nd:YAG solid-state four-level laser (532 nm) in  $180^\circ$  back-scattering geometry in conjunction with a monochromator (800 mm focal length) and Peltier-cooled CCD detector (Syncerity CCD, SYC0798-3316). The average acquisition time for a Raman spectrum was 3 min. Spectral resolution of  $1 \text{ cm}^{-1}$  was achieved with a grating of 1800 grooves  $\text{mm}^{-1}$ . Raman spectroscopic measurements were carried out on  $\text{Sm}_{0.5}\text{Y}_{0.5}\text{FeO}_3$  single crystal oriented along  $a$  and  $b$  axes in ambient condition. The schematic showing the orientation and polarization of the incident and scattered light on the (100) plane (plane  $\perp$  to  $a$  axis) of  $\text{Sm}_{0.5}\text{Y}_{0.5}\text{FeO}_3$  single crystal in standard Raman experiments is given in Fig. 1(a). The incident light from the laser source is polarized in a specific direction in the (100) plane while the scattered light is unpolarized. Figure 1(b) shows the orientation for the polarization studies in back-scattering geometry. Here, the direction of incident and scattered light was aligned parallel to [100] or [010] direction of the single-crystal sample using a rotator and analyzer to choose the polarization of the incident as

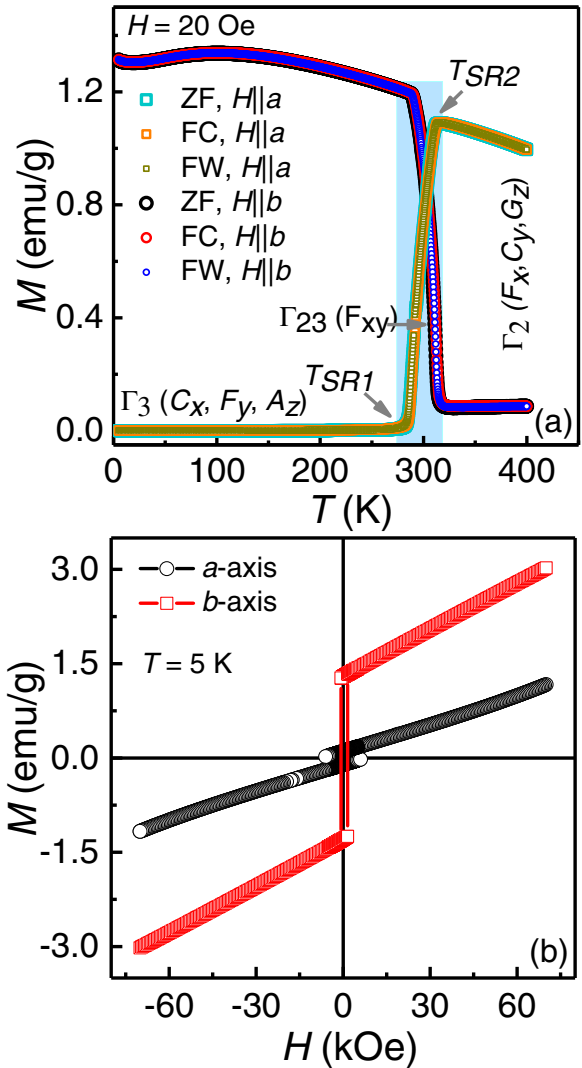


FIG. 2. (a) Magnetic moment,  $M(T)$ , of  $\text{Sm}_{0.5}\text{Y}_{0.5}\text{FeO}_3$  single crystal measured with  $H = 20$  Oe applied along the crystallographic axes  $a$  and  $b$ . ZF, FC, FW curves are shown. The cyan highlighted area marks the SR region where the transitions from  $\Gamma_2$  to  $\Gamma_3$  occur as temperature decreases. (b) Magnetization isotherms measured up to  $\pm 70$  kOe along  $a$  and  $b$  axes at 5 K.

well as the scattered light. Temperature-dependent Raman spectra were measured in a Linkam THMS 600 cryostage (Linkam Scientific, UK), equipped with a temperature controller (Linkam TMS 94), and a liquid-nitrogen pumping module (LNP 94) having an accuracy of  $\pm 0.1$  K. The spectra were recorded using LabSpec 6 software. The Lorentzian function was used to fit the profile of Raman modes and Gaussian profile for the two-magnon modes, after appropriate background subtraction.

## III. RESULTS AND DISCUSSIONS

Temperature-dependent magnetic moment of oriented single crystals ( $2 \times 2 \times 1 \text{ mm}^3$ ) was measured in the temperature range 5–400 K in zero-field (ZF), field-cooling (FC), and field-warming (FW) protocols by applying 20 Oe external magnetic field. Figure 2(a) shows the temperature dependence

of ZF, FC, and FW magnetic moment at 20 Oe along  $a(H \parallel a)$  and  $b(H \parallel b)$  axes of  $\text{Sm}_{0.5}\text{Y}_{0.5}\text{FeO}_3$  single crystal.

As the sample is cooled from 400 K, the weak FM moments of  $\text{Fe}^{3+}$  align along  $a$  axis until 312 K; as temperature decreases below 312 K, the weak FM moment rotates continuously from  $a$  to  $b$  axis and completely orients along the  $b$  axis at 282 K. This is synonymous with the spin reorientation transition of  $\text{Fe}^{3+}$  spins from  $a$  to  $b$  axis, marking the two transition temperatures  $T_{\text{SR}2} = 312$  K and  $T_{\text{SR}1} = 282$  K. A weak FM moment of  $\text{Fe}^{3+}$  persists along the  $a$  axis until Néel temperature ( $T_N = 654$  K) as shown in Fig. S3 of the Supplemental Material (SM) [11] (see, also, Refs. [12–15] therein). The parent  $\text{SmFeO}_3$  compound shows spin reorientation transition from  $c$  axis to  $a$  axis between  $T_{\text{SR}1} = 450$  K and  $T_{\text{SR}2} = 480$  K [1,9]. Whereas,  $\text{YFeO}_3$  does not show spin reorientation but the Fe moment is retained along the  $c$  axis from  $T_N = 645$  K to low temperature [1]. Generally, the rare-earth subsystem orders magnetically at very low temperature ( $T \leq 10$  K) and, above this temperature  $R^{3+}$  ions are paramagnetic and are polarized either parallel or antiparallel to the net  $\text{Fe}^{3+}$  moments by the  $R^{3+}$ - $\text{Fe}^{3+}$  magnetic interactions. When antiparallel, the net moment begins to decrease gradually which can be observed around 100 K in the total magnetic moment along  $b$  axis in Fig. 2(a). The  $\text{Sm}^{3+}$  sublattice is polarized antiparallel to the net  $\text{Fe}^{3+}$  moments in the molecular field of  $\text{Fe}^{3+}$  ions. [Here, the total magnetization  $M = F + (-m)$ , where  $F$  is the magnetization of Fe sublattice and  $m$  is magnetization of Sm sublattice.]  $\text{SmFeO}_3$  also exhibits this feature at 140 K [9].

The symmetry analysis of  $R\text{FeO}_3$  orthoferrites in orthorhombic  $Pbnm$  space group and for  $k = (000)$  propagation vector leads to eight possible irreducible representations (IR)  $\Gamma_1$  to  $\Gamma_8$  [1]. The symmetry-allowed spin configurations are shown in Table I. Among eight spin configurations,  $\Gamma_5$  to  $\Gamma_8$  are incompatible with the net moment at Fe sites, and hence not allowed. The remaining four spin configurations  $\Gamma_1(A_x, G_y, C_z)$ ,  $\Gamma_2(F_x, C_y, G_z)$ ,  $\Gamma_3(C_x, F_y, A_z)$ , and  $\Gamma_4(G_x, A_y, F_z)$  are possible in orthoferrites [1]. A previous report [1] suggests that  $\Gamma_3$  configuration is not consistent with strong AFM coupling between Fe nearest neighbors and hence not feasible in orthoferrites. However, due to weak ferromagnetic moment along the  $b$  axis, we have assigned a spin configuration of  $\Gamma_3$  in the present case. From the magnetization measurements along  $a$  and  $b$  axes, we rationalize that the magnetic structure transforms from canted antiferromagnetic with weak ferromagnetism along the  $a$  axis,  $\Gamma_2(F_x, C_y, G_z)$ , to weak ferromagnetic along the  $b$  axis,  $\Gamma_3(C_x, F_y, A_z)$ . The nonmagnetic nature and a smaller ionic radius of  $\text{Y}^{3+}$  (1.019 Å) in comparison to  $\text{Sm}^{3+}$  (1.079 Å) have a role in introducing structural distortions and altering the antisymmetric exchange to drive the spin reorientation process.

Doping  $\text{Y}^{3+}$  at  $\text{Sm}^{3+}$  site modifies the cell parameters (bond angle and bond length) mentioned in Table S1 of the SM [11] (see, also, Refs. [12–15] therein). Consequently, the relatively weak AFM coupling between  $\text{Fe}^{3+}$  sublattices establishes  $C$ -type and  $A$ -type AFM components along the  $a$  and  $c$  axes in preference to the  $G$ -type AFM component of stronger coupling strength. This marks the evolution of an unusual spin reorientation transition in  $\text{Sm}_{0.5}\text{Y}_{0.5}\text{FeO}_3$ ,  $\Gamma_2(F_x, C_y, G_z) \rightarrow \Gamma_{23}(F_{xy}) \rightarrow \Gamma_3(C_x, F_y, A_z)$  as temperature

TABLE I. The possible magnetic structures of  $R\text{FeO}_3$  allowed for  $Pbnm$  symmetry, where  $G$  denotes  $(+ - + -)$ ,  $F$   $(+ + + +)$ ,  $A$   $(+ - - +)$ ,  $C$   $(+ + - -)$ , and  $O$  (0000).  $G, F, C, A$ , and  $O$  are Bertaut's notation.  $x, y$ , and  $z$  denote orientations parallel to the crystallographic directions  $a, b$ , and  $c$ .

Irreps	Space group	$4b$	$4c$
$\Gamma_1$	$Pbnm$	$A_x G_y C_z$	$C_z$
$\Gamma_2$	$Pbn'm'$	$F_x C_y G_z$	$F_x C_y$
$\Gamma_3$	$Pb'nm'$	$C_x F_y A_z$	$C_x F_y$
$\Gamma_4$	$Pb'n'm$	$G_x A_y F_z$	$F_z$
$\Gamma_5$	$Pb'n'm'$	$O_x O_y O_z$	$G_x A_y$
$\Gamma_6$	$Pb'nm$	$O_x O_y O_z$	$A_z$
$\Gamma_7$	$Pbn'm$	$O_x O_y O_z$	$G_z$
$\Gamma_8$	$Pbnm'$	$O_x O_y O_z$	$A_x G_y$

decreases. The  $\Gamma_3$  spin configuration was recently observed in  $\text{Er}_{0.6}\text{Dy}_{0.4}\text{FeO}_3$  single crystal due to doped environment and modified lattice parameters [7]. An accurate determination of second-order anisotropy ( $K_2$ ) and fourth-order anisotropy ( $K_4$ ) constants will help in understanding the competition between the  $\Gamma_2$  and  $\Gamma_3$  phases and how the dynamics of spin reorientation transition changes as a function of temperature. This is most efficiently accomplished through terahertz spectroscopy [16], which is not within the scope of this work. Isothermal magnetization of  $\text{Sm}_{0.5}\text{Y}_{0.5}\text{FeO}_3$  as a function of the applied magnetic field,  $\pm 70$  kOe, along  $a$  and  $b$  axes at 5 K, after cooling from room temperature in zero fields are shown in Fig. 2(b). The weak ferromagnetic moment is aligned along the  $b$  axis of  $\text{Sm}_{0.5}\text{Y}_{0.5}\text{FeO}_3$  crystal at 5 K.

Raman spectroscopy is generally employed to study the magnetic transition in a sample to understand and correlate the underlying phenomena. Two strategies are used to investigate the SR transitions: (1) Tilt of  $\text{FeO}_6$  octahedra is a crucial structural parameter that regulates the physical properties by tuning the band structure. Probing the octahedral tilts and rotations (via associated vibrational modes) using Raman spectroscopy is a very reliable method to identify SR transitions, which are mediated through spin-phonon coupling [17–19]. (2) Raman spectroscopy is also an appropriate tool to study the inelastic scattering of light by single- and two-magnon excitations in single-crystal samples [20–25]. Magnon scattering can directly inquire about the spin properties of the system [20,24,25]. The phonon modes associated with the octahedral tilts of  $\text{Sm}_{0.5}\text{Y}_{0.5}\text{FeO}_3$  were probed by standard Raman spectroscopic measurements, carried out on the single-crystal samples oriented along  $a$  and  $b$  axes at ambient conditions (details given in Sec. II). The Raman spectra recorded for the (100) plane and (010) plane samples along with the Lorentzian peak fits are shown in Figs. 3(a) and 3(b), respectively. In orthorhombic perovskites, lattice dynamical calculations have assigned 24 Raman active modes:  $7A_{1g} + 7B_{1g} + 5B_{2g} + 5B_{3g}$  [26]. Between wave numbers 100 and  $700\text{ cm}^{-1}$ , we observed 12 Raman modes in both oriented (100) and (010) crystal planes. Modes below  $200\text{ cm}^{-1}$  are lattice modes characterized by motion of Sm/Y atoms. Modes between 200 and  $300\text{ cm}^{-1}$  are interpreted as due to  $\text{FeO}_6$  octahedral rotation while those between 300 and  $370\text{ cm}^{-1}$  are related to Sm-O (sharp

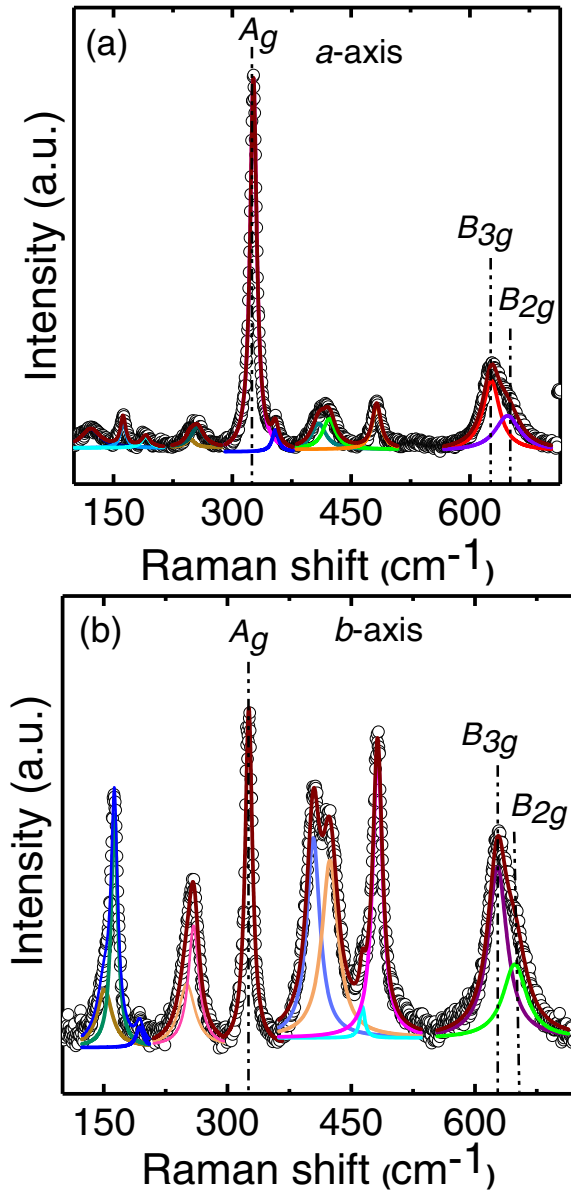


FIG. 3. Raman spectra of  $\text{Sm}_{0.5}\text{Y}_{0.5}\text{FeO}_3$  at 298 K measured for (a) (100) plane and (b) (010) plane along with the peak fit.

peak at  $325\text{ cm}^{-1}$ ) or Y-O vibrations [27]. Those between  $370$  and  $500\text{ cm}^{-1}$  yield various bending and antistretching modes of  $\text{FeO}_6$  octahedra [26,28]. The doublet with peaks at  $625$  and  $647\text{ cm}^{-1}$  is assigned to  $B_{3g}$  and  $B_{2g}$  modes for out-of-phase stretching and in-phase stretching of  $\text{FeO}_6$  octahedra, respectively [17,28,29]. The spectra for both crystal planes have most of the modes with similar peak positions except for one additional mode for (100) and (010) planes centered at  $354$  and  $463\text{ cm}^{-1}$ , respectively. However, the intensity ratio of all peaks varies substantially across the two planes. It is relevant to note that, for standard Raman spectroscopy, as the incident light is polarized, it interacts with vibrations only in specific directions of a single crystal. It manifests in the differences in the spectra when scattered in different directions, a behavior commonly observed in single crystals oriented in different planes [26,28,29].

Temperature-dependent Raman studies of  $\text{Sm}_{0.5}\text{Y}_{0.5}\text{FeO}_3$  single crystal for (100) and (010) planes were performed in the temperature range of  $80$ – $570\text{ K}$ . The evolution of spectra is shown in the stack plots of Figs. S5(a) and S5(b) in the SM [11] (see, also, Refs. [12–15] therein). It is observed that as the temperature increases, all the modes show a reduction of intensity. All of the modes are also exhibiting a softening except for the  $B_{2g}$  and  $B_{3g}$  modes. The spectra do not reveal any structural transition which is marked by sudden appearance or disappearance of peaks. This inference is consistent with the earlier studies on isostructural systems [20,28,29]. The peak positions of various modes of (100) and (010) planes were plotted against temperature. The temperature-dependent change in Raman shift of Sm-O stretching  $A_g$  mode measured between  $80$  and  $500\text{ K}$  is shown in Figs. 4(a) and 4(b). For a magnetic material, the temperature-dependent behavior of the phonon mode of frequency  $\omega(T)$  is given as [30]

$$\omega(T) = \omega_0 + (\Delta\omega)_{\text{latt}} + (\Delta\omega)_{\text{anh}} + (\Delta\omega)_{\text{ren}} + (\Delta\omega)_{\text{s-ph}}, \quad (1)$$

where  $(\Delta\omega)_{\text{latt}}$  is the shift in phonon frequency due to change in unit-cell parameters,  $(\Delta\omega)_{\text{anh}}$  is the contribution from intrinsic anharmonicity at constant volume,  $(\Delta\omega)_{\text{ren}}$  is the contribution from electronic state renormalization near the spin-ordering temperature (neglected for low carrier concentration), and  $(\Delta\omega)_{\text{s-ph}}$  is the spin-phonon coupling contribution by lattice vibration-induced modification of the exchange integral. Ideally, temperature-dependence phonon mode frequency  $\omega(T)$  should follow the anharmonic relation [Eqs. (S1) and (S2) of SM [11] (see, also, Refs. [12–15] therein)], resulting in a linear increase in the high-temperature regime, with decrease in temperature. For  $\text{Sm}_{0.5}\text{Y}_{0.5}\text{FeO}_3$  sample, most of the modes exhibit deviations from the linear trend near two temperatures:  $315$  and  $115\text{ K}$ . Expected linear behavior of hardening up to  $115\text{ K}$  with a subtle slope change near  $315\text{ K}$  is seen for  $A_g$  mode at  $325\text{ cm}^{-1}$  with the reducing temperature. Beyond  $115\text{ K}$ , the Raman shift has an opposite behavior and softens as temperature decreases, until  $80\text{ K}$ . This observation is similar in both oriented (100) and (010) crystal planes. In addition to the Sm-O stretching mode, peak position of various modes such as the  $B_{1g}$  mode corresponding to the  $R^{3+}$  ion motion at  $162\text{ cm}^{-1}$  and  $A_g$  modes around  $258\text{ cm}^{-1}$  [in (010) plane],  $355\text{ cm}^{-1}$  [in (100) plane],  $405\text{ cm}^{-1}$  [in (100) and (010) planes], and  $480\text{ cm}^{-1}$  [in (100) and (010) plane] show slope changes at  $315\text{ K}$  [Figs. S6 and S7 of SM [11] (see, also, Refs. [12–15] therein)]. Most of these peaks exhibit the anomaly near  $115\text{ K}$ . According to Eq. (1), these deviations from the linear behavior are attributed to the combined effect of other two components [ $(\Delta\omega)_{\text{latt}} + (\Delta\omega)_{\text{s-ph}}$ ] which are quasiharmonic effects and the spin-phonon coupling [19]. Further, explicit changes are observed in the peaks associated with the octahedral tilt, namely,  $B_{3g}$  and  $B_{2g}$  modes. Temperature dependence in the Raman shift of  $B_{2g}$  and  $B_{3g}$  modes (both planes) deviates from anharmonic dependence at two temperature points as evidenced by the anomalies; a small slope change at  $115\text{ K}$  and a second sharp change between  $310$  and  $320\text{ K}$  [Figs. 4(c) and 4(d)]. In the (100) plane, both  $B_{2g}$  and  $B_{3g}$  modes show hardening (opposite to the expected softening) with the increase of temperature from  $115$  to  $315\text{ K}$ , after which the modes begin to soften linearly until  $500\text{ K}$ . Interestingly, both  $B_{2g}$  and  $B_{3g}$  modes manifest opposite trends

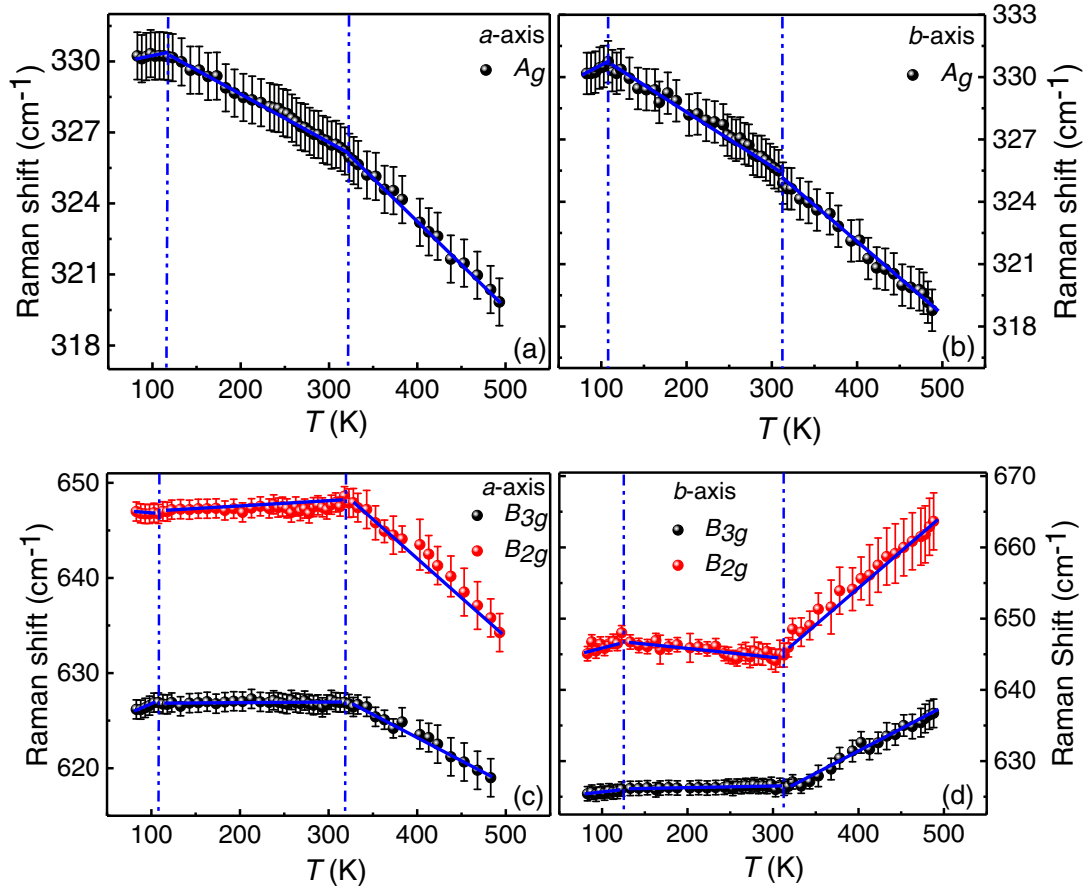


FIG. 4. Temperature dependence of Raman shift of  $A_g$  mode for (a) (100) plane and (b) (010) plane. Temperature dependence of Raman shift of the phonon modes  $B_{3g}$  and  $B_{2g}$  for (c) (100) and (d) (010) planes. Solid blue lines are guide to the eye. Dashed blue vertical lines represent deviations from a linear slope for temperature dependence of Raman shift.

in the (010) plane. As expected, there is softening of both modes in the temperature range between 115 and 315 K, but this is followed by hardening until 500 K. In consonance with the magnetic studies, the anomalies in various Raman modes around 315 K are found to be the signature of SR transition, marking the  $T_{SR2}$  value. Nevertheless, it is significant to note that the  $B_{2g}$  and  $B_{3g}$  modes behave differently across the two different planes, during the temperature variation, while most of the other modes show a very similar trend along both axes. Here, the deviation in Raman shift during SR transition is unprecedentedly stronger than commonly observed changes, and shows a clear distinction across different planes, indicating the clear anisotropic nature in the changes of the magnetic moments during the transition. Anomalies in the peak position in the vicinity of SR transitions have been reported previously in Raman studies of magnetic materials [17–19]. The origin of such anomalies was explained by Chaturvedi *et al.* [19] by performing temperature-dependent x-ray diffraction (XRD) in  $\text{SmFeO}_3$ . They observed nonlinear changes in the lattice parameters near  $T_{SR}$ . Changes in lattice parameters and volume were also reflected in the Raman shift of the material [18,19]. Similar trends in the peak position of various modes of  $\text{Sm}_{0.5}\text{Y}_{0.5}\text{FeO}_3$  suggest nonlinearity in lattice parameters due to exchange striction driven spin coupling. The anomaly in the peak shift of most Raman modes near 115 K is a signature of the antiparallel ordering of samarium in the exchange

field of Fe, as evidenced by the magnetization measurement. Similar observations are reported by Weber *et al.* in  $\text{SmFeO}_3$  single crystal [31], where they attributed the anomalies to the suppression of magnetic moment. High-temperature studies have revealed a change of slope due to the substantial drop in intensity of  $B_{3g}$  and  $B_{2g}$  modes in (100) and (010) planes, respectively, at 505 K. These are highlighted in Fig. S9 of SM [11] (see, also, Refs. [12–15] therein). From the magnetic studies, it is clear that the changes near this temperature do not have a magnetic origin. The origin of these changes are also discussed in the SM [11] (see, also, Refs. [12–15] therein).

Changes in spin-phonon coupling due to external parameters affect the lifetime of the phonons and are identified through Raman linewidth analysis. In a crystalline material, Raman linewidth is inversely proportional to the lifetime of phonon modes. The effect of temperature on full-width at half-maxima (FWHM) of  $B_{2g}$  and  $B_{3g}$  modes of  $\text{Sm}_{0.5}\text{Y}_{0.5}\text{FeO}_3$  crystal in (100) and (010) planes are illustrated in Fig. 5. According to the anharmonic relation describing the temperature dependence of linewidth [Eq. (S2) in SM [11] (see, also, Refs. [12–15] therein)], the linewidth is expected to decrease with decreasing temperature in high-temperature regime. Deviation from this behavior is observed in the case of FWHM of  $B_{3g}$  and  $B_{2g}$  modes for both (100) and (010) planes. Figures 5(a) and 5(c) show the change in FWHM of  $B_{3g}$  and  $B_{2g}$  modes, respectively, along the  $a$  axis. FWHM value of  $B_{3g}$

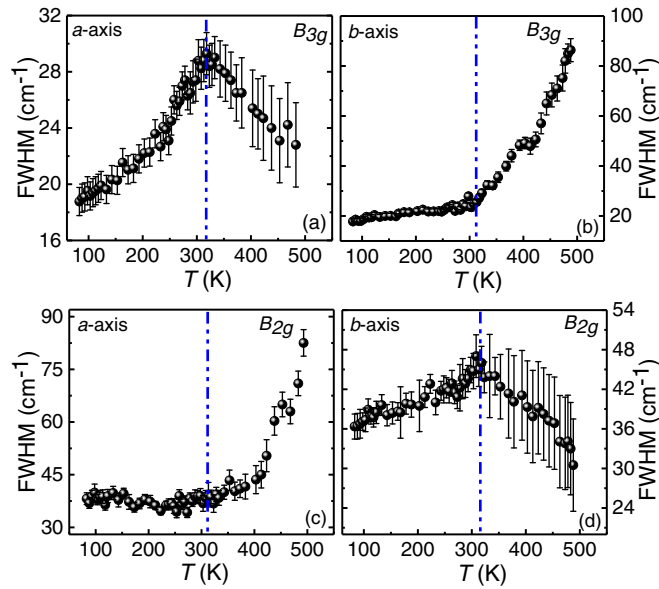


FIG. 5. FWHM changes with temperature for (a)  $B_{3g}$  mode of (100) plane and (b) (010) plane, and (c)  $B_{2g}$  mode of (100) plane and (d) (010) plane of  $\text{Sm}_{0.5}\text{Y}_{0.5}\text{FeO}_3$  crystal. Dashed blue vertical lines represent anomalous points.

mode increases with decreasing temperature until SR transition (315 K). Below 315 K, it decreases linearly until 80 K as expected. Whereas FWHM of  $B_{2g}$  mode decreases as expected until the SR transition, below which there is a plateau in the temperature range of 315–115 K. In case of  $B_{3g}$  and  $B_{2g}$  modes along the  $b$  axis [Figs. 5(b) and 5(d)], the trend in change of FWHM with temperature is different. Here,  $B_{3g}$  mode is almost stagnant below the SR transition, where the  $B_{2g}$  mode shows the opposite behavior. These changes indicate the noncollective rotation of Fe ion spins due to the competition of the two magnetic structures, leading to a change in spin-phonon coupling and phonon lifetime. The changes in FWHM help us to understand that the anomalies in Raman shift is in fact indicative of the SR transition via spin-phonon coupling and negate the possibility of structural transition or magnetostriction. FWHM does not show a change of trend near 115 K, but only marginal changes in the slope, which is almost insignificant with the error bar. These changes could also be the result of variations in spin-phonon coupling during the change of  $\text{Sm}^{3+}$  magnetic moment.

There have been numerous studies on rare-earth orthoferrites (polycrystalline samples or single crystals that have grown in a specific direction) that cite spin reorientation transitions corroborated by the slope change in Raman shift and FWHM of various modes [18,28]. Our study is focused on specific Raman modes with off-diagonal components of polarizability ( $B_{3g}$  and  $B_{2g}$ ) that can interact with the canted AFM spin in the  $\text{Sm}_{0.5}\text{Y}_{0.5}\text{FeO}_3$  through spin-phonon coupling. The contrasting behaviors in the temperature dependence of both Raman shift and FWHM in the  $B_{3g}$  and  $B_{2g}$  modes across the two planes having axes parallel to the spin direction is remarkable. To understand how the spin-phonon coupling causes structural changes in magnetic materials, Mochizuki *et al.* [32] have proposed a theoretical model. They have analyzed the

role of spin-phonon coupling in  $\text{RMnO}_3$  which has helped to interpret the phase transitions in several magnetic materials including orthoferrites [19]. According to this model, with temperature the  $\text{Fe}^{3+}\text{-Fe}^{3+}$ ,  $\text{Y}^{3+}\text{-Fe}^{3+}$ , and  $\text{Sm}^{3+}\text{-Fe}^{3+}$  interactions favor the displacement of  $\text{Sm}^{3+}$  and  $\text{Y}^{3+}$  ions in  $\text{Sm}_{0.5}\text{Y}_{0.5}\text{FeO}_3$ , to minimize the distortion of  $\text{FeO}_6$  octahedra. It is interesting to note that the  $A_g$  mode ( $325 \text{ cm}^{-1}$ ) corresponding to Sm-O vibration shows only a slight slope change [Figs. 4(a) and 4(b)]. Also, the mode corresponding to  $R^{3+}$  ion motion follows the linear trend between 115 and 500 K in both FWHM and Raman shift, with a slope change at 315 K [Figs. S7(a)–S7(d) of SM [11] (see, also, Refs. [12–15] therein)]. The relatively small changes in modes involving the  $R^{3+}$  ion, compared to the octahedral modes indicate the cause-effect nature of Sm displacement and resulting changes in  $\text{FeO}_6$  octahedra. The trilinear coupling of  $\text{Fe}^{3+}$  and  $\text{Sm}^{3+}$  spins and the octahedral tilt systems modifies the Fe-O-Sm coupling path inducing changes in magnetic moments [31]. The  $R$  ion displacement leads to significant polar lattice distortion resulting in a relatively large polarization and change in magnetic spin direction around the observed transition temperature of 315 K. We infer from the Raman data that the displacements retain the strength of  $B_{2g}$  and  $B_{3g}$  modes along  $a$  and  $b$  axes, respectively, until the SR transition. Afterwards, the displacement occurs in the opposite direction, indicating the clear involvement of exchange striction in the SR transition. It is also inferred that the spin-phonon coupling reduces the phonon lifetime of  $B_{2g}$  mode substantially in the (100) plane and that of  $B_{3g}$  mode in the (010) plane with an accompanying sharp increase in FWHM of these modes in the corresponding axes. In contrast, the clear change of trend in FWHM and peak position near 115 K for the modes below  $400 \text{ cm}^{-1}$  is a distinct sign of changes in  $\text{Sm}^{3+}$  sublattice due to the alignment of Sm spins.

Some previous studies have focused on Raman spectroscopy of magnon scattering in which magnon peaks were used to interpret the spin properties and SR transitions [20,24,25]. This technique was barely applied for ferroic samples due to the weak intensity of magnon scattering compared to that of phonon scattering. This problem has been addressed by selecting the appropriate polarization configuration to enhance the intensity of the magnon modes. The polarized Raman spectra and the two-magnon mode across different polarization configurations are shown in Fig. 6. The two-magnon mode was observed with promising intensity in the cross polarizations  $\bar{x}(y, z)x$  and  $\bar{y}(z, x)y$  centered at  $950 \text{ cm}^{-1}$ . This is in agreement with the previously reported results of isostructural systems [20,23,25]. Magnon peaks with high intensity in crossed polarization were earlier reported in similar samples having large Raman cross section of magnon scattering in specific configurations [25]. A sudden decline in the intensity of magnon peaks at specific polarization is known to be a signature of the SR transition [20,25]. This is apparent from the stack plots in Figs. 7(a) and 7(c). By analogy, we tag the sharp fall in two-magnon scattering intensity to SR transition starting at 280 K in both the cross-polarization configurations. The integrated area under the two-magnon curves was plotted against temperature as shown in Figs. 7(b) and 7(d). A sharp decrease in the intensity is visible between 270 and 350 K. From the polarization-dependent studies, it has shown that the

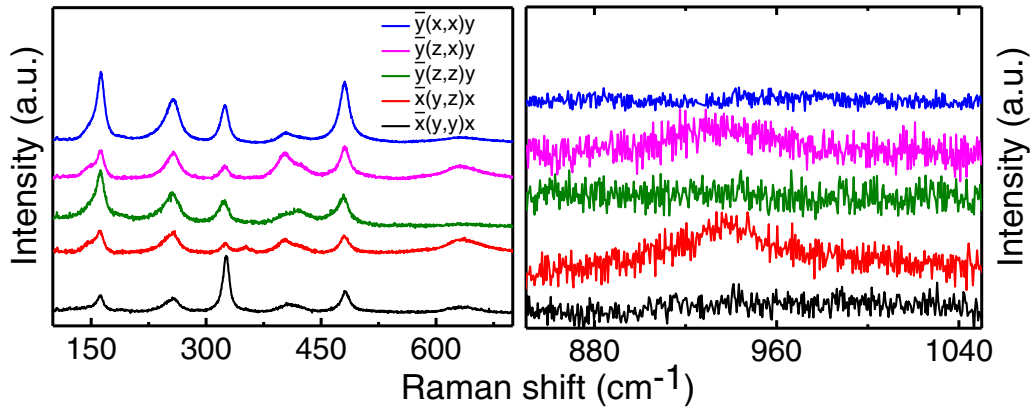


FIG. 6. Polarized Raman spectra of  $\text{Sm}_{0.5}\text{Y}_{0.5}\text{FeO}_3$  single crystal at 295 K from 100 to 1050  $\text{cm}^{-1}$  in different polarization configurations enhancing the two-magnon modes.

two-magnon peak is highly anisotropic and obtained only in specific configurations [Fig. 6(b)]. The changes in the direction of the magnetic symmetry greatly influence the intensity

of the magnon mode as shown in previous studies [25]. The intensity is drastically reduced until 350 K and remains constant thereafter. The stack plot of 2M mode in normal Raman at

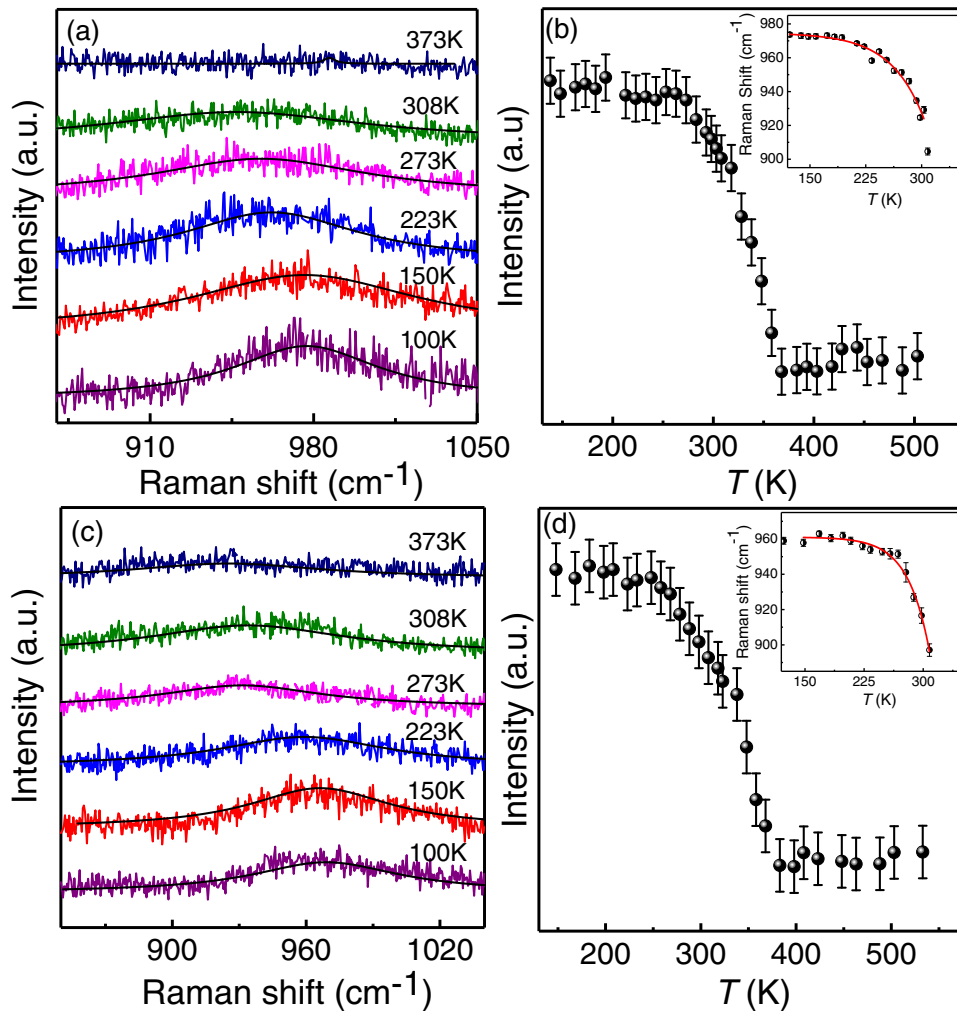


FIG. 7. (a) Temperature-dependent (100–373 K) polarized Raman showing two-magnon modes in  $\bar{x}(y, z)x$  configuration. (b) Temperature dependence of the integrated area under the two-magnon curve and inset shows temperature dependence of peak position of two-magnon mode in  $\bar{x}(y, z)x$  configuration. (c) Temperature dependent (100–373 K) polarized Raman spectra of two-magnon mode in  $\bar{y}(z, x)y$  configuration. (d) Temperature dependence of the integrated area under the two-magnon curve and inset shows temperature dependence of peak position of two-magnon mode in  $\bar{y}(z, x)y$  configuration. Red solid line in insets of (b) and (d) is the guide to eye showing the nonlinear trend.

various temperatures is shown in Fig. S10(a) of SM [11] (see, also, Refs. [12–15] therein) for comparison. Without specific polarization, the intensity of the magnon mode is much lower than that in the polarization study. However, the peaks could be fitted until higher temperatures (450 K), after which the Gaussian profile is lost in the background [the two-magnon peaks have very low intensity and were practically absent in the normal Raman spectra of (010) plane, thus, it was not possible to study the evolution with temperature]. The integrated intensity of two-magnon peaks from normal Raman scattering measurements was also plotted against temperature and shown in the Fig. S10(b) of SM [11] (see, also, Refs. [12–15] therein). When compared with the integrated intensity plots of two-magnon modes from polarization studies, the intensity of the peak from normal Raman spectra shows only a gradual decrease. The reduction in intensity occurs in the range from 250 K until 450 K, where the Gaussian features disappears. While the result of the normal Raman is more consistent with previous studies [25], the polarization studies indicate the transition more clearly. It is also evident from this comparison that the anisotropic nature of the two-magnon peak is one of the major reasons for the dramatic drop of intensity in polarization studies. Inset of Figs. 7(b) and 7(d) illustrate the temperature dependence of two-magnon peak position until 310 K. Further, the two-magnon mode softens in a nonlinear manner with a sharp drop from  $T_{SR1}$  (at 275 K) as temperature is increased. The softening of magnon modes associated with the SR transition was also reported previously [20,21].

The transition temperatures deduced from Raman study do not limit to a specific range in most cases except those for the two-magnon modes. This is at variance with the values derived from magnetization studies where the start and the end of the SR transition range is clearly defined. It is important to realize that Raman shift is not a direct reflection of the magnetic changes, but the interaction of these changes with the vibrations in the system. Hence, in the case of Raman measurement, with the lowering temperature, various anomalies are observed at the beginning of SR transition. Beyond this temperature, the spin-phonon coupling associated with SR transition does not undergo a major change, hence, we do not see any change in Raman data at 282 K. Additionally, Chaturvedi *et al.* has reported a change in the linearity of the lattice parameters and Raman shift in the upper limit of SR transition, when plotted against temperature, for isostructural system  $\text{SmFeO}_3$

[19]. Considering the similarities in structure and properties, it is logical to assume the same in the case of  $\text{Sm}_{0.5}\text{Y}_{0.5}\text{FeO}_3$ . Further, the two-magnon modes which are not associated with the structural changes, also show marked changes in both the upper and lower limits of the SR transition. This is evident in the intensity and peak position plots in Figs. 7(b) and 7(d). There is a slight mismatch between the transition temperature obtained in the Raman spectroscopic study and that from magnetization measurement. This is due to the dependence of SR transitions on the applied magnetic field in the case of magnetization measurement but remains independent for the temperature-dependent Raman method.

#### IV. CONCLUSIONS

In summary, this study reveals an unusual temperature-induced spin reorientation transition from  $\Gamma_2$  to  $\Gamma_3$  spin configuration near room temperature, in the interval of 282–312 K. The weak ferromagnetic moment of  $\text{Fe}^{3+}$  remains along the  $a$  axis until Néel temperature ( $T_N = 654$  K). Our studies reveal the potential of  $\text{Sm}_{0.5}\text{Y}_{0.5}\text{FeO}_3$  system to be a vital material in spintronic devices due to room-temperature spin reorientation transition. The striking changes associated with the Raman modes in temperature-dependent Raman studies confirm the reorientation of spin lattice structure, specifically, the weak ferromagnetic component reorienting from  $b$  to  $a$  axis. Additionally, magnon-spectral peaks observed in polarized Raman investigations reaffirm the reorientation of spin configuration and the anisotropy associated with the transition. Temperature-dependent Raman data reveal the involvement of strong spin-phonon coupling via exchange striction in driving the unusual SR transition in  $\text{Sm}_{0.5}\text{Y}_{0.5}\text{FeO}_3$  single crystal.

#### ACKNOWLEDGMENTS

Financial support from University Grants commission (UGC-531996), India, for Senior research fellowship (B.M.) and Department of Science and Technology (S.E.) through Core Research Grant are gratefully acknowledged. Authors acknowledge Dr. P. Yanda, Professor A. Sundaresan, CPMU, JNCASR for high-temperature magnetic measurements.

B.M. and J.S. contributed equally to this work.

- 
- [1] R. L. White, *J. Appl. Phys.* **40**, 1061 (1969).  
 [2] A. V. Kimel, A. Kirilyuk, A. Tsvetkov, R. V. Pisarev, and T. Rasing, *Nature (London)* **429**, 850 (2004).  
 [3] A. V. Kimel, B. A. Ivanov, R. V. Pisarev, P. A. Usachev, A. Kirilyuk, and T. Rasing, *Nat. Phys.* **5**, 727 (2009).  
 [4] Y. Tokunaga, S. Iguchi, T. Arima, and Y. Tokura, *Phys. Rev. Lett.* **101**, 097205 (2008).  
 [5] A. I. Belyaeva and K. V. Baranova, *Bull. Russian Acad. Sci: Phys.* **73**, 1056 (2009).  
 [6] U. Staub, L. Rettig, E. M. Bothschafter, Y. W. Windsor, M. Ramakrishnan, S. R. V. Avula, J. Dreiser, C. Piamonteze, V.

- Scagnoli, S. Mukherjee, C. Niedermayer, M. Medarde, and E. Pomjakushina, *Phys. Rev. B* **96**, 174408 (2017).  
 [7] J. Li, L. Jiang, H. Chen, L. Su, E. D. Mishina, N. E. Sherstyuk, S. N. Barilo, and A. Wu, *Appl. Phys. Lett.* **116**, 192409 (2020).  
 [8] Y. K. Jeong, J.-H. Lee, S.-J. Ahn, and H. M. Jang, *Solid State Commun.* **152**, 1112 (2012).  
 [9] J.-H. Lee, Y. K. Jeong, J. H. Park, M.-A. Oak, H. M. Jang, J. Y. Son, and J. F. Scott, *Phys. Rev. Lett.* **107**, 117201 (2011).  
 [10] X. Lin, J. Jiang, Z. Jin, D. Wang, Z. Tian, J. Han, Z. Cheng, and G. Ma, *Appl. Phys. Lett.* **106**, 092403 (2015).



- [11] See Supplemental Material at <http://link.aps.org/supplemental/10.1103/PhysRevB.105.214417> for the single-crystal growth and its structural characterization.
- [12] S. Ding, M. Xue, Z. Liang, Z. Liu, R. Li, S. Cao, Y. Sun, J. Zhao, W. Yang, and J. Yang, *J. Phys.: Condens. Matter* **31**, 435801 (2019).
- [13] I. Fita, A. Wisniewski, R. Puzniak, V. Markovich, and G. Gorodetsky, *Phys. Rev. B* **93**, 184432 (2016).
- [14] I. Fita, A. Wisniewski, R. Puzniak, E. E. Zubov, V. Markovich, and G. Gorodetsky, *Phys. Rev. B* **98**, 094421 (2018).
- [15] M. Balkanski, R. F. Wallis, and E. Haro, *Phys. Rev. B* **28**, 1928 (1983).
- [16] K. Yamaguchi, T. Kurihara, Y. Minami, M. Nakajima, and T. Suemoto, *Phys. Rev. Lett.* **110**, 137204 (2013).
- [17] P. Mandal, V. S. Bhadram, Y. Sundarayya, C. Narayana, A. Sundaresan, and C. N. R. Rao, *Phys. Rev. Lett.* **107**, 137202 (2011).
- [18] A. A. Khan, A. Ahlawat, P. Deshmukh, M. Singh, A. Sagdeo, V. Sathe, A. Karnal, and S. Satapathy, *J. Alloys Compd.* **885**, 160985 (2021).
- [19] S. Chaturvedi, P. Shyam, A. Apte, J. Kumar, A. Bhattacharyya, A. M. Awasthi, and S. Kulkarni, *Phys. Rev. B* **93**, 174117 (2016).
- [20] N. Koshizuka and S. Ushioda, *Phys. Rev. B* **22**, 5394 (1980).
- [21] S. Venugopalan, M. Dutta, A. K. Ramdas, and J. P. Remeika, *Phys. Rev. B* **31**, 1490 (1985).
- [22] S. Sugai, S.-i. Shamoto, and M. Sato, *Phys. Rev. B* **38**, 6436 (1988).
- [23] N. Koshizuka and K. Hayashi, *J. Phys. Soc. Jpn.* **57**, 4418 (1988).
- [24] T. M. H. Nguyen, T. H. Nguyen, X.-B. Chen, Y. Park, Y. M. Jung, D. Lee, T. Noh, S.-W. Cheong, and I.-S. Yang, *J. Mol. Struct.* **1124**, 103 (2016), special Issue: Novel Developments and Applications of Two-Dimensional Correlation Spectroscopy.
- [25] X.-B. Chen, N. T. M. Hien, K. Han, J.-Y. Nam, N. T. Huyen, S.-I. Shin, X. Wang, S. W. Cheong, D. Lee, T. W. Noh *et al.*, *Sci. Rep.* **5**, 13366 (2015).
- [26] M. C. Weber, M. Guennou, H. J. Zhao, J. Íñiguez, R. Vilarinho, A. Almeida, J. A. Moreira, and J. Kreisel, *Phys. Rev. B* **94**, 214103 (2016).
- [27] S. Tyagi, V. Sathe, G. Sharma, M. Gupta, R. Mittal, V. Srihari, and H. K. Poswal, *Mater. Chem. Phys.* **215**, 393 (2018).
- [28] S. Gupta, R. Medwal, S. P. Pavunny, D. Sanchez, and R. S. Katiyar, *Ceramics International* **44**, 4198 (2018).
- [29] Y. S. Ponosov and D. Y. Novoselov, *Phys. Rev. B* **102**, 054418 (2020).
- [30] E. Granado, A. García, J. A. Sanjurjo, C. Rettori, I. Torriani, F. Prado, R. D. Sánchez, A. Caneiro, and S. B. Oseroff, *Phys. Rev. B* **60**, 11879 (1999).
- [31] M. C. Weber, M. Guennou, D. M. Evans, C. Toulouse, A. Simonov, Y. Kholina, X. Ma, W. Ren, S. Cao, M. A. Carpenter *et al.*, *Nat. Commun.* **13**, 443 (2022).
- [32] M. Mochizuki, N. Furukawa, and N. Nagaosa, *Phys. Rev. B* **84**, 144409 (2011).